P-Type 3C-SiC photocathode for Solar to Hydrogen Energy Conversion

Masashi Kato

Department of Electrical & Mechanical Engineering, Nagoya Institute of Technology, Gokiso, Showa, Nagoya 466-8555, Japan

Silicon carbide (SiC) is a chemically stable and photocatalytic semiconductor material. Among SiC polytypes, 3C-SiC has the smallest band gap (2.3 eV), and thus 3C-SiC is capable to absorb a significant part of solar light. The use of p-type semiconductor as photocathode reduces hydrogen in water. Cathodic operation prevents oxidation of photocatalytic materials. Therefore p-type 3C-SiC will be an efficient and durable photocatalyst. Our experiments have revealed that p-type 3C-SiC acts as photocathodes with excellent performance. Solar to hydrogen conversion efficiency for p-type 3C-SiC photocathodes with Pt cocatalysts was 0.52 %. Considering such a high efficiency and possibility of further improvement, SiC is a very promising material for the solar to hydrogen conversion technology.

Introduction

Solar to hydrogen energy conversion technologies attract attention as renewable energy generation. To perform solar to hydrogen conversion, photocatalytic reaction and water splitting with semiconductor materials are widely employed. However, most of photocatalytic materials are oxide semiconductors and they cannot absorb visible light resulting in low conversion efficiencies (1-3). Photocatalysts other than oxide semiconductors are usually corrode and degrade during operation (4). Thus, we need to find new photocatalysts which have both high conversion efficiencies and resistance to corrosion.

Silicon carbide (SiC) is a chemically stable semiconductor material and acts as a photocatalyst (5). SiC can be grown by different atomic configurations resulting in a large number of polytypes (5-7). The band gaps of SiC depends on the polytypes, and they range from 2.3 to 3.2 eV, which are larger than a fundamental energy for water splitting 1.23 eV, and SiC will have potential to split water. Among SiC polytypes, 3C-SiC has the smallest band gap, 2.3 eV, and thus 3C-SiC is capable to absorb significant part of solar light. In addition, conductive type of SiC can be controlled by impurity doping. Photoelectrodes based on photocatalysts with p-type conduction operate as cathode and reduce hydrogen in water. Cathodic operation prevents oxidation of photocatalytic materials. Therefore, p-type 3C-SiC is expected as an efficient and durable photocatalyst.

Considering the potential of SiC as a photocatalyst described above, we have experimentally characterized various SiC crystals by fabrication and measurements of photoelectrode structures (6-10). In this paper, we reviewed our experimental findings for

SiC photoelectrodes, and, in particular for p-type 3C-SiC photocathodes, we discussed possibility of SiC for application of solar-to-hydrogen energy conversion.

Capability of water splitting by SiC

Theoretical solar-to-hydrogen conversion efficiency η can be calculated using experimentally observed optical absorption coefficients (11) and assumption of one photon creating one electron to reduce one hydrogen ion (100% Faradic efficiency). The calculated results for a structure with flat surface (without any light confinement structure) are shown in Figure 1. η depend on thickness of the layer for optical absorption, because SiC has indirect band gaps and significant amount of photons penetrate SiC. 3C-SiC with 30 μm thickness will have η > 5%, while other polytypes will show less than 2% because of the large band gaps.

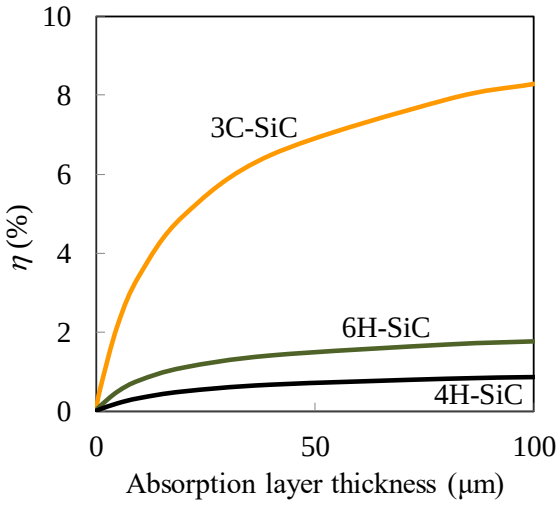

Figure 1. Theoretically-estimated optical absorption layer thickness dependence of solar-to-hydrogen energy conversion efficiencies η for 3C-, 6H- and 4H-SiC.

To perform water splitting by semiconductor photocatalysts, the semiconductor must have a band gap straddling the hydrogen reduction and water oxidation potentials. We have confirmed the band edge potentials for SiC polytypes from Mott-Schottky plots of capacitance voltage (*C*-*V*) characteristics using SiC photoelectrodes against a saturated calomel electrode (SCE) as shown in Figure 2 (6). We also show the redox potentials of H_2/H^+ and H_2O/O_2 as the top and bottom of the gray band. Even though, the conduction band edge of 3C-SiC is near to the hydrogen reduction potential, all the SiC polytypes show capability of water splitting.

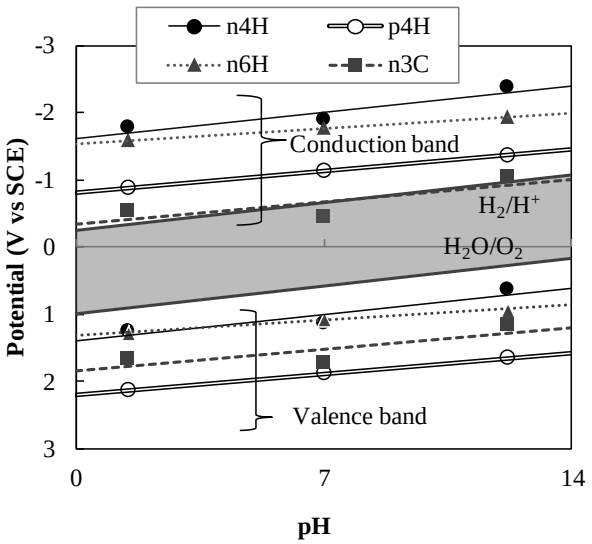

Figure 2. Band edge potentials of SiC in various pH. The redox potentials of H_2/H^+ and of H_2O/O_2 are also indicated by the top and bottom lines of the gray band.

Conductivity type, polytype and crystalline quality

We have measured photocurrent in aqueous solution with potential control by a potentiostat using SCE as a reference electrode. For samples, sublimation grown bulk crystal and epitaxial layer grown by chemical vapor deposition (CVD) were employed.

Figure 3 shows the time dependence of photocurrents under light illumination of 1 W/cm^2 from a solar simulator for the n-type SiC. The electrolyte was 1M H_2SO_4 aqueous solution which is a typical electrolyte for hydrogen generation (12-14) and applied potential was 0 V vs SCE. In this case, because the samples were n-type, SiC photoelectrodes acted as photoanode and oxidation reaction proceeds on the SiC surface. The photocurrents were observed for all n-type SiC but they decreased gradually. It is known that n-type SiC is oxidized by light illumination in an electrolyte (15-17), and resulting SiO_2 behaves as a resistant layer for photocurrent. By the Auger electron spectroscopy, we confirmed formation of an oxide layer on epitaxial n-type 4H-SiC, which shows the largest photocurrent among n-type samples. Therefore, the decrease of photocurrent for the n-type samples would be caused by SiO_2 formation.

Figure 4 shows photocurrents for the p-type SiC photoelectrode, which acts as photocathodes in electrolytes. The photocurrents do not significantly decrease with time, and the photocurrent of the epitaxial 4H-SiC is larger than those of bulk samples as in the case of n-type samples. No oxide formation or corrosion was observed for the p-type SiC after the photocurrent measurements in an optical micrograph and a surface profile by a profilometer. In addition, large photocurrents are observed on the epitaxial 4H-SiC compared with the bulk SiC for both n- and p-type. We have then employed epitaxially-grown p-type 4H-, 6H- and 3C-SiC layers for all experiments after this finding.

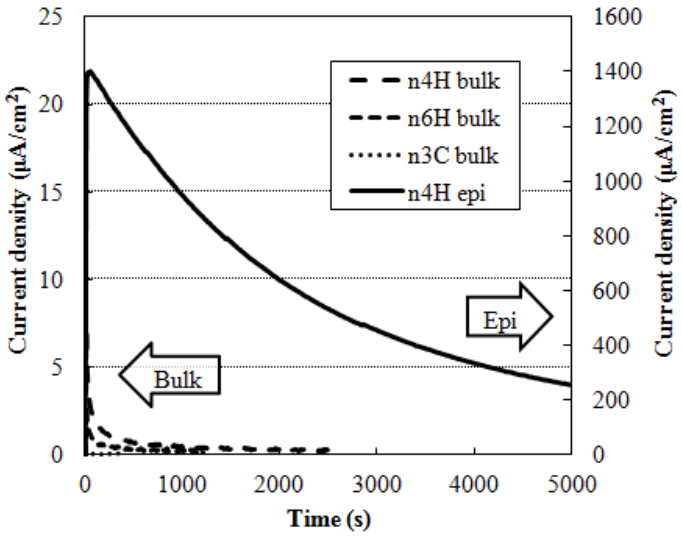

Figure 3. Time dependence of photocurrents under 1 W/cm^2 light illumination in the aqueous 1 M H_2SO_4 solution for the n-type SiC with a three-electrode system at which potential of 0 V vs SCE was applied to SiC.

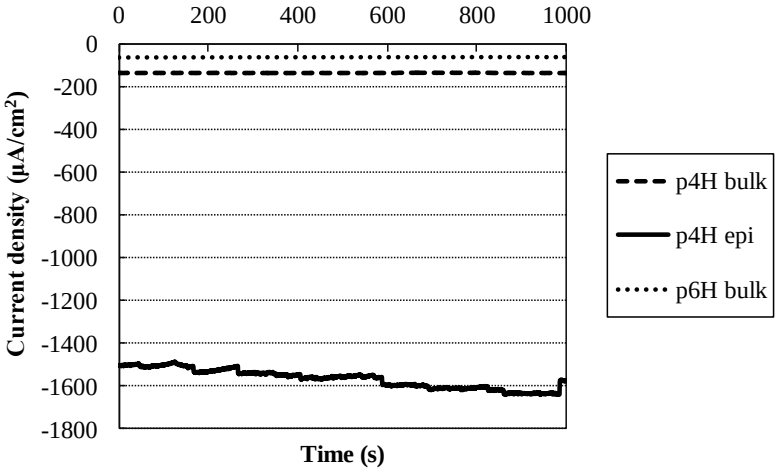

Figure 4. Time dependence of photocurrents under 1 W/cm^2 light illumination in the aqueous 1 M H_2SO_4 solution for the p-type SiC with a three-electrode system at which potential of 0 V vs SCE was applied to SiC.

In the three-electrode system, external electrical power is supplied from a potentiostat to stabilize the potential in SiC. Therefore, experiments using the two electrode-system are required to see potential for solar-to-hydrogen conversion. Figure 3 shows the time dependence of photocurrents for epitaxially-grown p-type 4H- (p4H), 6H- (p6H) and 3C-SiC (p3C) layers in the two-electrode system using either Pt or Ni as counter electrodes without external bias. When Pt was used as a counter electrode, the photocurrents were very small compared to those obtained in the three-electrode system. These results suggest that the adjustment of the potential difference between Pt and the electrolyte by the potentiostat enhances the photocurrent. On the other hand, with the Ni counter electrode, the measured photocurrents are larger than those obtained in the same system with the Pt electrode. The photocurrents are constant and seem to depend on the band gap of the SiC polytypes, 3C-SiC has the smallest band gap and exhibits the largest photocurrent among all the samples.

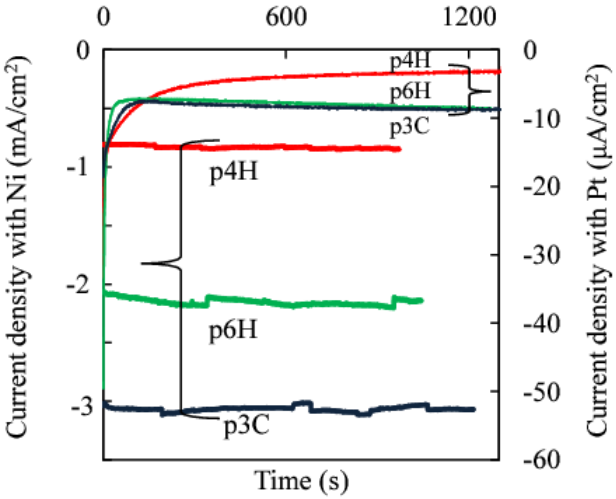

Figure 5. Time dependence of photocurrents for p4H, p6H and p3C in aqueous H_2SO_4 solution with the two-electrode system using Pt or Ni counter electrodes.

To understand effects of crystalline quality, we have measured carrier lifetimes τ and depletion layer widths W for various SiC samples. For photocatalytic operation of photoelectrodes, the photogenerated electrons must reach the electrolyte. Therefore, when the diffusion length of electrons L_D, which is proportional to square root of τ, and W in the photocathode are large, electrons excited deep inside of the photocathode can contribute to the reaction as in solar cells, i.e., a photocathode is active for wavelengths near to that corresponding to the band gap energy, at which absorption coefficient α of the material is small.

Here, we show experimental results of $L_D + W$ and photocurrents for 4H-SiC samples. Control of τ and impurity doping concentration is relatively easy for this polytype and thus experimental data for 4H-SiC are abundant compared with those for other polytypes. τ were measured by using the microwave photoconductivity decay (μ-PCD) method, and from τ we estimated $L_D = (D_e \cdot \tau)^{0.5}$ by using the diffusion coefficients D_e calculated from the Einstein's relationship and the reported electron mobilities μ_e (26, 2.6, and 26 cm^2/s for 4H-, 6H-, and 3C-SiC, respectively (18)). On the other hand, W was estimated by capacitance at 0 V vs SCE in 1 M H_2SO_4 aqueous solution. Photocurrents observed with

the same electrolyte with the samples illuminated by 1 W/cm^2 solar light using the three-electrode system with 0V vs SCE or the two-electrode system with Ni. Observed photocurrents are shown in Figure 6 against $L_D + W$. The photocurrents by the two and three electrode systems monotonically depend on $L_D + W$. In this figure, we also show the line for theoretical calculation by integration of photons absorbed within $L_D + W$ (photon integral), which is based on an assumption that all the absorbed photons is converted to photocurrent. We also calculated photocurrents using an one dimensional device simulator AMPS-1D for solar cell structure with a Schottky barrier (19). These calculations also show a monotonical dependence of photocurrents on $L_D + W$.

Usually τ and resulting L_D are large for high quality crystals, while W is large when impurity doping density is low. Therefore, from the results shown in Figure 6, we considered that high crystalline quality and low impurity doping density are desirable for performance improvement of SiC photocathodes.

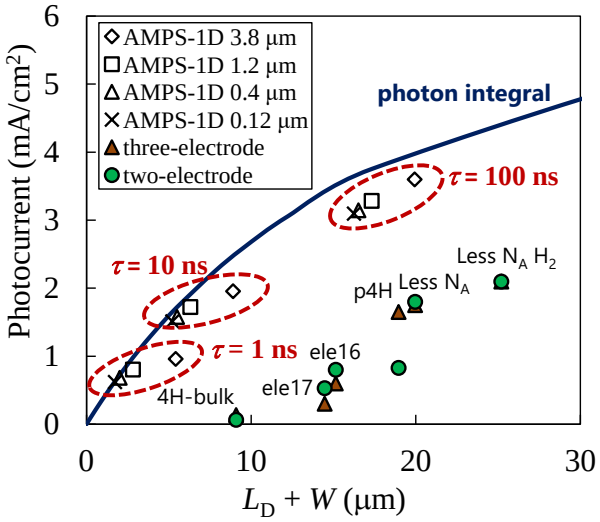

Figure 6. Dependence of photocurrent on the sum of diffusion length L_D and depletion layer width W for the 4H-SiC samples (4H-bulk, ele17, ele16, p4H, Less N_A and Less N_A H_2). The shaded symbols are experimental results. The line and unshaded symbols are calculated by photon integration and AMPS-1D with various carrier lifetime τ and W values, respectively (values of W are indicated in the legend).

Improvement of 3C-SiC crystalline quality

As noted earlier, 3C-SiC is a most promising polytype to obtain high η. However, bulk crystal growth of 3C-SiC is very difficult because this polytype is stable only in growth at much lower temperature than sublimation of SiC, which is a typical condition for bulk SiC growth. Therefore, unlike hexagonal 4H- and 6H-SiC, free-standing 3C-SiC substrates are not industrially produced. This situation makes that 3C-SiC can be grown only by CVD on Si or 4H- or 6H-SiC substrates. When Si is used as a substrate, generation of crystal defects due to a difference in lattice constant cannot be avoided. When SiC substrate is used, there is almost no difference in lattice constant, so generation of crystal defects can be avoided. However, on SiC substrates with (0001) face with off-angle, which is common substrates in the SiC substrate market, the growth layer is formed by the step flow mechanism and inherits the polytype of the substrate (5,20). Therefore, the SiC substrate on the (0001) on-axis surface is suitable for 3C-SiC growth.

To obtain high quality 3C-SiC crystals, we have recently chosen CVD growth on 4H-SiC substrates, because 3C polytype is relatively stable on on-axis (0001) Si-face of 4H-SiC substrates (5,17). In fact, 3C-SiC we employed up to this point had been grown on 6H-SiC substrates because on-axis (0001) substrates are typically produced by 6H polytypes from various substrate vendors. For our recent 3C-SiC photocathode fabrication, we employed p^+-type 4H-SiC substrates with the (0001) Si-face inclined 0.7° to <1120> direction. Growth on the 4H-SiC substrates with quasi on-axis Si-face prevents polytype mixing and p^+-type conductivity of the substrate facilitates ohmic contact formation on the substrate side. We performed 3C-SiC growth on the substrates by CVD with silane and propane as source gases and in an Al acceptor doping condition. Al doping density was suppressed as low as possible with keeping p-type conductivity. A photograph of the grown crystal is shown in Figure 7(a).

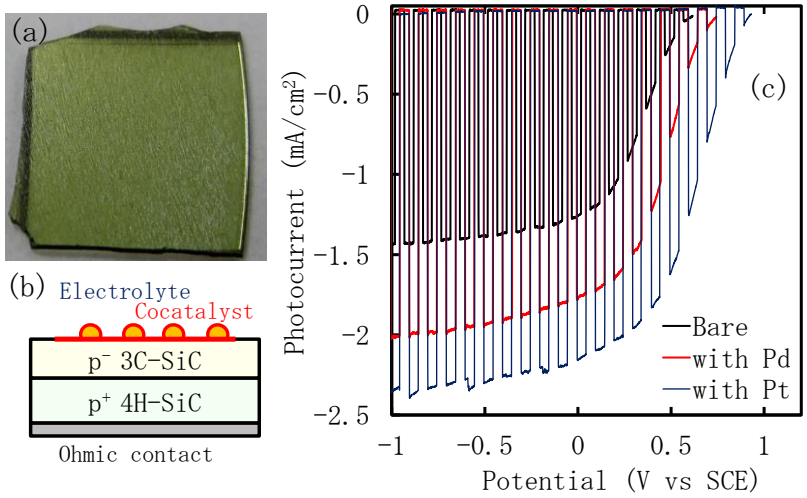

Figure 7. (a) Photograph of p-type 3C-SiC grown on 4H-SiC, (b) schematic of the photocathode structure using p-type 3C-SiC grown on 4H-SiC, and (c) photocurrent-potential characteristics at 100 mW/cm^2 light power for photocathodes using p-type 3C-SiC grown on 4H-SiC w/o (Bare) and w/ Pd or Pt cocatalysts.

Figures 8(a) and 8(b) show optical micrographs for the surfaces of 3C-SiC grown on 4H-SiC and 3C-SiC grown on 6H-SiC, respectively. For 3C-SiC grown on 4H-SiC, the surface has macro steps parallel to the <1 $\bar{1}$00> direction with uniform yellowish color. For 3C/6H, there are domains with two colors: yellowish and white colors. This result indicates two different domains (3C-SiC and 6H-SiC) in 3C-SiC grown on 6H-SiC. From Raman spectroscopy measurements, we identified that the yellowish region was 3C-SiC while the white region was 6H-SiC, and 58% of the surface area for 3C-SiC grown on 6H-SiC corresponds to 3C-SiC. On the other hand, the entire surface of 3C-SiC grown on 4H-SiC is 3C polytype.

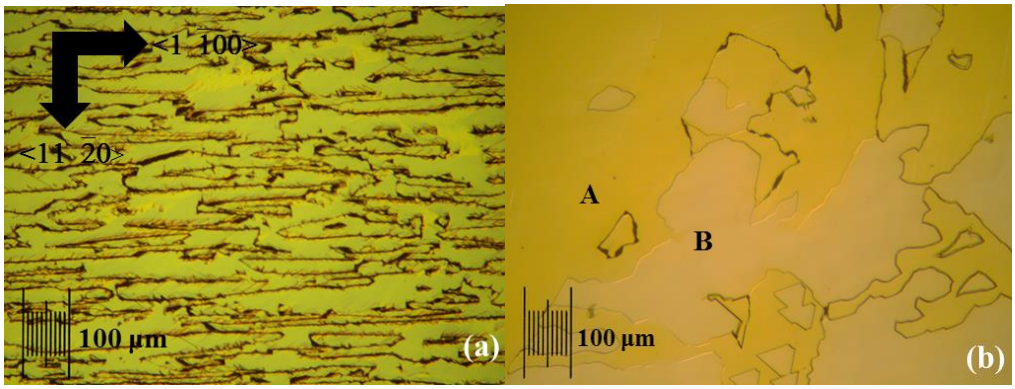

Figure 8. Optical micrograph for the surfaces of (a) 3C-SiC grown on 4H-SiC and (b) 3C-SiC grown on 6H-SiC.

We fabricated ohmic contacts on the substrate side of 3C-SiC grown on 4H-SiC. The 3C-SiC surface is active surface as the photocathode. In addition, we formed Pt or Pd cocatalysts on the 3C-SiC surface to enhance hydrogen generation. The detail of the cocatalyst formation is described in nest section. The schematic of the photocathode structure is shown in Figure 7(b).

We measured photocurrent-potential characteristics for the 3C-SiC on 4H-SiC photocathodes in 1 M H_2SO_4 aqueous solution using chopped solar simulator light with 100 mW/cm^2. The results are shown in Figure 7(c). For bare surface, cathodic photocurrent was observed below 0.6 V vs SCE, and it reached –1.4 A/cm^2 at –1 V vs SCE. The light power was 1/10 compared with experiments shown in Figures 3-6, while this photocurrent of –1.4 A/cm^2 was almost half those obtained from conventional p-type 3C-SiC as shown in Figure 5 (–3 A/cm^2). Therefore, photocurrents obtained from 3C-SiC grown on 4H-SiC increased by factor of five from conventional 3C-SiC.

Cocatalyst formation and solar-to-hydrogen conversion

The observed photocurrent from the 3C-SiC on 4H-SiC photocathodes is still smaller than the theoretical expectation. Therefore, performance of the 3C-SiC photocathodes should be improved further. One of the methods for improving the performance of photoelectrodes is formation of cocatalysts, which reduce the overpotential of photoelectrodes in the redox reaction, on photoelectrode surfaces (21,22). It has been shown that Pt or Pd particles behave as cocatalysts on photocathodes, and they enhances the H_2 production efficiency for photocatalytic water splitting (23,24). Therefore, we formed Pt or Pd particles as cocatalysts on a surface of the 3C-SiC on 4H-SiC photocathodes. Pt cocatalysts was formed by an electrochemical deposition method using an aqueous solution of 0.05 M H_2PtCl_6 and 1 M HCl with deposition current of –800 µA/cm^2 at 40 ºC (25). On the other hand, Pd cocatalysts was formed by a photochemical deposition method (26). In this paper, the details are described only for the Pt cocatalyst formation process because of its better performance.

Figure 9 shows the time dependence of photocurrents using 1 W/cm^2 light for the bare surface and after the Pt cocatalysts formation processes of 10-60 s. The rise and fall of photocurrents were caused by change in the reaction area. The photocurrents were fell

by reduction of the reaction area due to the adherence the generated hydrogen bubbles, while the photocurrents were raise by increase of the reaction area due to the removal of generated hydrogen bubbles. As shown in this figure, the photocurrents depended on the periods of the Pt cocatalysts formation process, and the photocathode after the 50 s Pt formation process resulted in the largest photocurrent.

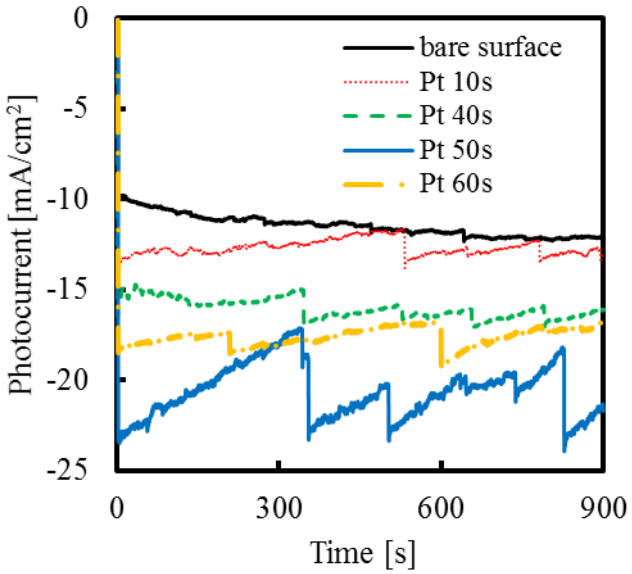

Figure 9. Time dependence of full-spectrum photocurrents in aqueous H_2SO_4 solution with the two-electrode system using Ni counter electrode illuminated with 1 W/cm^2 solar light for the bare surface and after the Pt cocatalysts formation processes of 10-60 s,

Figure 10 shows the AFM images (1.7 μm × 1.7 μm) for the bare surface and after the Pt cocatalysts formation. Particles were not observed on the bare surface, while particles were observed on the surface after the Pt cocatalysts formation. The particle size became larger, as the period of the Pt cocatalysts formation process is increased.

Photocurrent-potential characteristics for the 3C-SiC on 4H-SiC photocathodes with Pt and Pd cocatalysts are shown in Figure 7(c). Photocurrents from the photocathode with cocatalysts were observed at higher potential compared with the bare surface. Pt cocatalysts were more effective than Pd cocatalysts, and in the case of with Pt cocatalysts, photocurrent was observed from 0.9 V vs SCE and was –2.3 A/cm^2 at –1 V vs SCE. Such the photocurrents are comparable to the photocurrent using the other best photoelectrode materials (27,28).

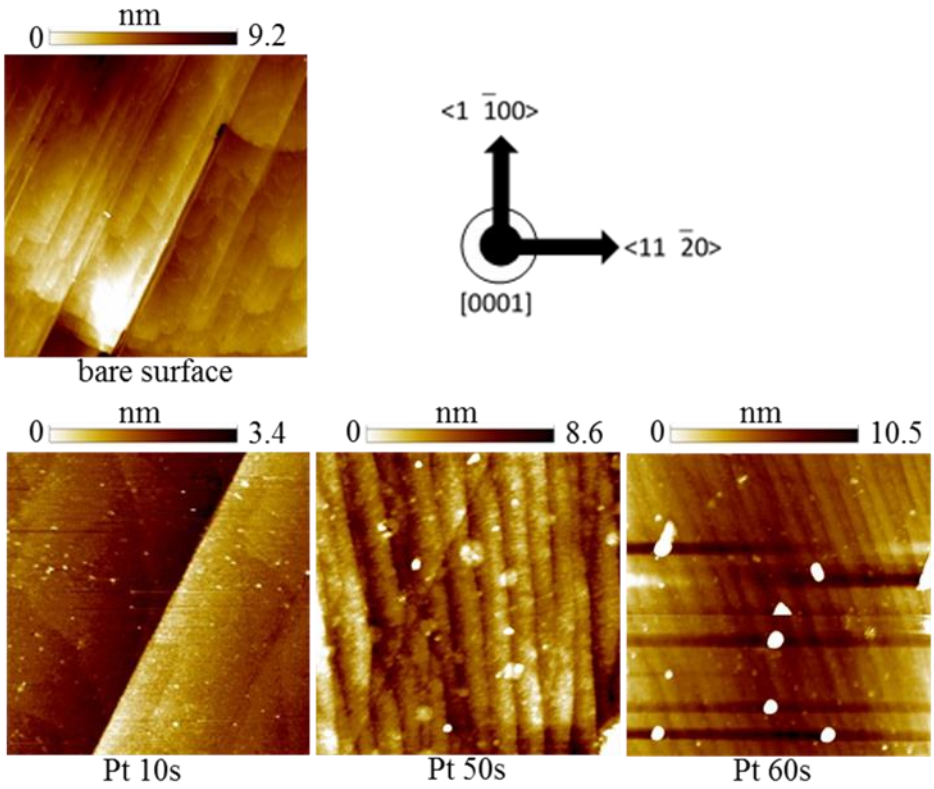

Figure 10. AFM images (1.7 × 1.7 μm) for the bare surface and after the Pt cocatalysts formation processes of 10-60 s

Figure 11 shows the hydrogen volumes generated by photocathodes in aqueous H_2SO_4 solution with the two-electrode system using the Ni counter electrode illuminated with 1 W/cm^2 solar light to the bare surface, after the 50s Pt and 120s Pd cocatalysts formation processes. The plots indicate the hydrogen volumes measured by gas chromatography, whereas the lines indicate the hydrogen volumes estimated from the integration of the photocurrents. The integrations of the photocurrents were almost linear, which indicates that the photocathodes were not degraded during the experiments. The measured hydrogen volumes are almost the same as the estimations by the photocurrents. This results indicates that the Faraday efficiencies of the photocathodes were near to 100%. The photocathode after the 50s Pt cocatalysts formation process shows maximum hydrogen volumes as expected from the photocurrent-potential characteristics. Appearance of hydrogen production can be browsed on our website http://ik-lab.web.nitech.ac.jp/SiC/photosynthesis.html.

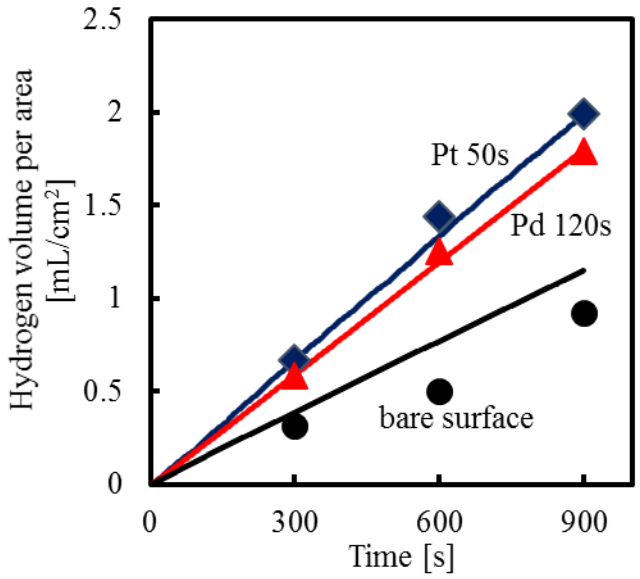

Figure 11. Hydrogen volumes generated from photocathodes in aqueous 1M H_2SO_4 solution with the two-electrode system using the Ni counter electrode illuminated with 1 W/cm^2 solar light for the bare surface, after the 50s Pt and 120s Pd cocatalysts formation processes. The plots indicate the volumes measured by gas chromatography, and the lines indicate estimations from the photocurrents.

We performed photocurrent-voltage measurements with RuO_2 as a counter electrode to estimate η. RuO_2 is a stable material against oxidation and has a low oxygen overpotential, and thus we can estimate accurate η by using the RuO_2 counter electrode. Figure 12 shows photocurrent-voltage curves with a RuO_2 counter electrode for the bare surface, after the 50s Pt and 120s Pd cocatalysts formation processes. We estimated the η from the maximum power point. The voltage sweep rate of 5 mV/s and light power was 1 W/cm^2 in aqueous 1M H_2SO_4 solution. For the bare surface, η was 0.21 % at –0.98 V vs RuO_2. After the 120s Pd cocatalysts formation process showed 0.46 % at –0.84 V vs RuO_2, while after the 50s Pt cocatalysts formation process showed 0.52 % at –0.78 V vs RuO_2. η of 0.52 % is comparable to the photocurrent using other best photoelectrode materials (27-31). We have never seen degradation of the SiC photocathode performance even after repeated experiments, and thus the SiC photocathodes are a durable for long-term hydrogen energy generation.

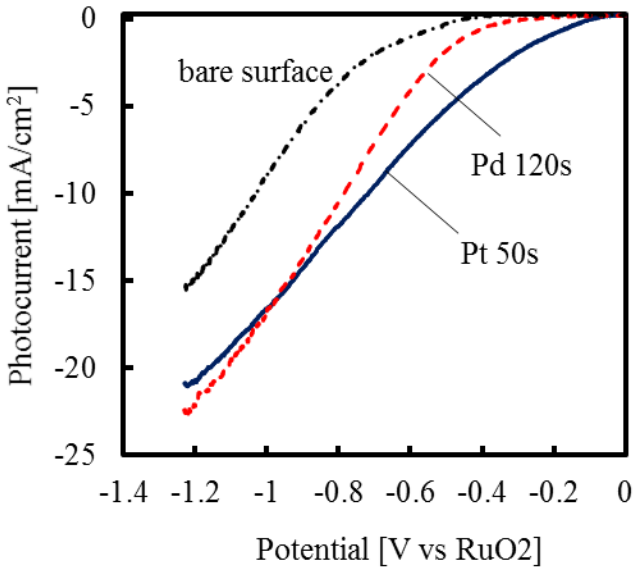

Figure 12. Photocurrent-voltage curves for the bare surface, after the 50 s Pt and 120 s Pd cocatalysts formation processes in aqueous 1 M H_2SO_4 solution with the two-electrode system using the RuO_2 counter electrode illuminated with 1 W/cm^2 solar light.

Conclusion

We have dedicated to see possibility of SiC for application of solar-to-hydrogen conversion. We have characterized SiC samples various polytypes and conductivity, and discussed importance of crystalline quality. Then we found that high quality p-type 3C-SiC crystals are the best for this application among SiC crystals. Photocathodes fabricated by p-type 3C-SiC shows nearly 100% Faraday efficiency and they were not degraded during solar-to-hydrogen conversion experiments. η for the p-type 3C-SiC photocathodes with Pt cocatalysts was 0.52 %. Considering such a high efficiency and durability, SiC is a very promising material for the solar to hydrogen conversion technology. Furthermore, we have recently found other methods to obtain η higher than 0.52 % using 3C-SiC photocathodes and the methods will be reported in future.

Acknowledgments

This work is supported by Grant-in-Aid for Scientific Research 25107516 and 15H00872, the Naito Science and Engineering Foundation, the JGC-S Scholarship Foundation, the Takahashi Industrial and Economic Research Foundation, the Tatematsu Foundation and the Adaptable and Seamless Technology Transfer Program, Japan Science and Technology Agency. The author thanks his students Tomonari Yasuda, Keiko Miyake and Naoto Ichikawa, and Prof. Masaya Ichimura, Prof. Tomoaki Hatayama and Dr. Takeshi Ohshima.

References

1. S. U. M. Khan, M. Al-shahry, and W. B. Ingler, Jr., *Science* **297**, 2243 (2002).
2. C. Das, P. Roy, M. Yang, H. Jha, and P. Schmuki, *Nanoscale* **3**, 3094 (2011).
3. R. S. Pessoa, M. A. Fraga, L. V. Santos, M. Massi, and H. S. Maciel, *Mater. Sci. Semicond. Process.* **29**, 56 (2015).
4. A. W. Mau, C. Huang, N. Kakuta, A. J. Bard, A. Campion, M. A. Fox, J. M. White, and S. E. Webber, *J. Am. Chem. Soc.* **106**, 6537 (1984).
5. T. Kimoto, A. Itoh, and H. Matsunami, *Phys. Status Solidi (b)* **202**, 247 (1997).
6. T. Yasuda, M. Kato, M. Ichimura, and T. Hatayama, *Appl. Phys. Lett*., **101**, 53902 (2012).
7. M. Kato, T. Yasuda, K. Miyake, M. Ichimura, and T. Hatayama, *Int. J. Hydrogen Energy*, **39**, 4845 (2014).
8. N. Ichikawa, M. Kato, and M. Ichimura, *Appl. Phys. Express*, **10**, 091301 (2015).
9. M. Kato, K. Miyake, T. Yasuda, M. Ichimura, T. Hatayama, and T. Ohshima, *Jpn. J. Appl. Phys.*, **55**, 01AC02 (2016).
10. N. Ichikawa, M. Kato, and M. Ichimura, *Appl. Phys. Lett.*, **109**, 153904 (2016).
11. S.G. Sridhara, T.J. Eperjesi, R.P. Devaty, W.J. Choyke, *Mat. Sci. Eng.* **B61-62**, 229 (1999)
12. I. Lauermann, R. Memming, and D. Meissner, *J. Electrochem. Soc.* **144** (1997) 73.
13. K. Fujii and K. Ohkawa, *J. Electrochem. Soc.* **153**, A468 (2006).
14. J. Akikusa and S. U. M. Khan, *Int. J. Hydrogen Energy* **27**, 863 (2002).
15. J. O. M. Bockris and K. Uosaki, *J. Electrochem. Soc*. **124**, 1348 (1977)
16. M. Kato, M. Ichimura, and E. Arai, *Jpn. J. Appl. Phys.* **40**, L1145 (2001).
17. M. Kato, M. Kimura, and M. Ichimura, *Jpn. J. Appl. Phys.* 52, 04CP02 (2013).
18. O. Madelung ed. *Data in Science and Technology, Semiconductors Group IV Elements and III–V Compounds* (Springer, Berlin 1991).
19. http://www.ampsmodeling.org/
20. K. Kojima, H. Okumura, S. Kuroda, and K. Arai, *J. Cryst. Growth* **269**, 367 (2004).
21. J. T. Song, T. Iwasaki and M. Hatano, *Jpn. J. Appl. Phys.* **54**, 04DR05 (2015).
22. M. G. Walter, E. L. Warren, J. R. McKone, S. W. Boettcher, Q. Mi, E. A. Santori and N. S. Lewis, *Chem. Rev.* **110**, 6446 (2010).
23. Y. Wang, Y. Wang and R. Xu, *J. Phys. Chem. C* **117**, 783 (2013).
24. M. Ye, J. Gong, Y. Lai, C. Lin and Z. Lin, *J. Am. Chem. Soc.* **134**, 15720 (2012).
25. M. E. Baumgartner and Ch. J. Raub, *Platinum Metals Rev.* **32**, 188 (1988).
26. M. Ichimura and T. Sueyoshi, *Jpn. J. Appl. Phys.* **48**, 015503 (2009).
27. R. Saito, Y. Miseki and K. Sayama, *Chem. Commun.* **48**, 3833 (2012).
28. M. Seki, M. Takahashi, T. Ohshima, H. Yamahara and H. Tabata, *Jpn. J. Appl. Phys.* **53**, 05FA07 (2014).
29. T. Bak, J. Nowotny, M. Rekas, and C. Sorrell, *Int. J. Hydrogen Energy* **27**, 991 (2002).
30. L. Zhang, T. Minegishi, M. Nakabayashi, Y. Suzuki, K. Seki, N. Shibata, J. Kubota, and K. Domen, *Chem. Sci.* **6**, 894 (2015).
31. M.M. May, H.-J. Lewerenz, D. Lackner, F. Dimroth, and T. Hannappel, *Nat. Commun.* **6**, 8286 (2015).